# Dynamic stall model modifications to improve the modeling of vertical axis wind turbines

**Pirrung, Georg; Gaunaa, Mac**

*Publication date:*
2018

*Document Version*
Publisher's PDF, also known as Version of record

# Dynamic stall model modifications to improve the modeling of vertical axis wind turbines

Georg R. Pirrung and Mac Gaunaa

June 2018

Report Number: DTU Wind Energy E-0171

ISBN: 978-87-93549-39-5

DTU Vindenergi
Institut for Vindenergi

**Author(s):** G. R. Pirrung and M. Gaunaa
**Title:** Dynamic stall model modifications to improve the modeling of vertical axis wind turbines
**Institute:** Department of Wind Energy

**Summary:**
The Beddoes-Leishman type dynamic stall model was originally implemented in HAWC2 with a focus on horizontal axis wind turbines.
In case of HAWTs, some terms in the unsteady airfoil lift and drag are very small and can be neglected, which are very important for VAWTs.
Furthermore, the angle of attack variations during normal operation of VAWTs are by far larger than those occuring on HAWTs. This posed a challenge to the Beddoes-Leishman-type dynamic stall model, which had previously been validated for small variations in angle of attack against CFD and measurements.
This report contains some necessary modifications of the Beddoes-Leishman type dynamic stall model in HAWC2 to enable unsteady aerodynamic computations on VAWTs. A short validation against measurements of the NREL/NASA Ames Phase VI rotor in standstill is included. There, it is shown that the model changes have only a small, but beneficial effect at small angle of attack variations.

**Report Number:** DTU Wind Energy E-0171
**Publication Date:** June 2018

**ISBN:** 978-87-93549-39-5

Technical University of Denmark
DTU Wind Energy
Frederiksborgvej 399
4000 Roskilde
Denmark

# Contents

# 1 Introduction

The Beddoes-Leishman type dynamic stall model implemented in HAWC2 is described in [1]. It has been developed with the horizontal axis wind turbine in mind. In case of the horizontal axis wind turbine, some added mass terms from thin airfoil theory can be neglected. Further, the angle of attack (AOA) variations are typically small in normal operation. In standstill, where the AOA variations could be large because the complete relative flow at the airfoil is affected by turbulence, the blades can be in deep stall where the current dynamic stall model is not valid anyway. Therefore previous validations in [1] and [2] have been mainly concerned about small angle of attack variations.

The blades of vertical axis turbines (VAWTs) see much larger variations in AOA during normal operation, especially at high wind speeds. Further, lift and drag contributions depending on the torsion rate or the acceleration of the airfoil perpendicular to the chord become large and have to be included in the modeling.

This report describes some modifications and extensions to the Beddoes-Leishman type dynamic stall model implemented in HAWC2. These modifications concern the attached flow part of the model. The scaling of shed vorticity in the attached flow angle of attack lag presented in the report has been developed by Pirrung and Gaunaa in March 2016. The additional contributions due to torsion rate and acceleration are mainly based on the appendix in Peter Bæks PhD thesis [3].

# 2 Original model description

The present report does not go into detail about the stall part of the dynamic stall model, because all the extensions and modifications in this report concern the attached flow part. Briefly, the dynamic stall part works as follows:

- two polars are generated based on the input polar: a linear attached flow polar and a nonlinear separated flow polar
- the separation point position $f_{sep}$ is used to interpolate between the polars.
  - $f_{sep} = 1$ means the separation point is at the trailing edge. The flow is fully attached.
  - $f_{sep} = 0$ means the separation point is at the leading edge. The flow is fully separated.
- a time lag is applied to the separation point position to model unsteady behavior of the flow separation ('dynamic stall').

The attached flow part models a lagging of the 'effective' angle of attack $\alpha_E$ behind the geometric angle of attack at the three quarter chord point $\alpha_{3/4}$:

$$\alpha_E = \alpha_{3/4}(1 - A_1 - A_2) + \frac{x_1}{U} + \frac{x_2}{U}, \quad \text{everything at time } t \tag{1}$$

$$x_i(t) = x_i(t - \Delta t)e^{b_i \Delta t / T_0} + \frac{1}{2}(\alpha_{3/4}(t - \Delta t) + \alpha_{3/4}(t))A_i U(t)(1 - e^{b_i \Delta t / T_0}), \tag{2}$$

where $A_i$ and $b_i$ are factors of Jones' indicial (impulse-response) function

$$\Phi(s) = 1 - A_1 e^{-b_1 s} - A_2 e^{-b_2 s} \tag{3}$$

The time constant $T_0$ is defined as $T_0 = c/(2U)$ with the chord length $c$ (half chord $b$) and the relative velocity $U$.

An attached flow lift coefficient $c_{l,att,E}$ and a separated flow lift coefficient $c_{l,sep,E}$ are determined by interpolating the airfoil polars at $\alpha_E$. The 'circulatory' (for lack of a better term) lift

coefficient is then determined by interpolation between attached and separated lift coefficient based on the separation point position $f_{sep}$, [1]:

$$c_{l,circ} = c_{l,att,E} f_{sep} + c_{l,sep,E}(1 - f_{sep}) \tag{4}$$

Another contribution to the lift coefficient, that follows directly from thin airfoil theory, is the 'torsion rate lift':

$$c_{l,tors} = \pi T_0 \dot{\theta} \tag{5}$$

The total lift coefficient is the sum of the components above:

$$c_l = c_{l,circ} + c_{l,tors} \tag{6}$$

The drag coefficient has three contributions: a contribution that follows from the polar at the efficient angle of attack, $c_{d,E}$, a contribution due to separation $c_{d,sep}$ and an induced drag component$c_{d,ind}$, see [1]. The induced drag is due to the change in lift direction between the effective and geometric angle of attack and vanishes in steady state.

$$c_{d,ind} = c_l(\alpha_{3/4} - \alpha_E) \tag{7}$$

$$c_d = c_{d,E} + c_{d,sep} + c_{d,ind} \tag{8}$$

# 3 Extended model description

## 3.1 Attached flow angle of attack lag

The original dynamic stall model produced very large AOA lags for VAWTs operating at high wind speeds, cf. Section 4.1. These large lags occur because the attached flow angle of attack lag is computed as if the airfoil was in attached flow continously. Because the angle of attack lag is caused by vorticity shed from the trailing edge of the airfoil due to the variation in bound circulation, this effect should not occur in stall to the same degree as in attached flow.

To adress this issue, the indicial function based algorithm for the angle of attack has been rewritten into a version, where the new contributions to the angle of attack lag can easily be scaled:

$$\alpha_E = \alpha_{3/4} - \frac{x_1}{U} - \frac{x_2}{U}, \quad \text{everything at time } t \tag{9}$$

$$x_i(t) = x_i(t - \Delta t) e^{b_i \Delta t / T_0} + (w_{3/4}(t) - w_{3/4}(t - \Delta t)) \frac{A_i}{b_i} \frac{T_0}{\Delta t} (1 - e^{b_i \Delta t / T_0}) f_{scale} \tag{10}$$

$$w_{3/4} = \alpha_{3/4} U, \tag{11}$$

where $w_{3/4}$ is the induced downwash at the three quarter chord point. If the scaling function $f_{scale} = 1$, this algorithm performs almost identically as the original algorithm above. Choosing the separation point position of the previous time step effectively removes additional shed vorticity in full stall and thus reduces the predicted AOA lags:

$$f_{scale} = f_{sep}(t - \Delta t) \tag{12}$$

The modified model with the separation point position as scaling factor behaves virtually the same way as the original model in attached flow.

## 3.2 Torsion rate and acceleration contributions

The additional terms introduced in this section are based on [3].

Due to the circular motion of VAWT blades, the airfoils see a constant acceleration $\ddot{y}$ perpendicular to the chord towards the center of rotation, which contributes to the lift coefficient:

$$c_{l,acc} = -\pi T_0 \frac{\ddot{y}}{U} \tag{13}$$

The full lift coefficient is obtained as:

$$c_l = c_{l,circ} + c_{l,tors} + c_{l,acc} \tag{14}$$

$$\tag{15}$$

With $c_{l,circ}$ and $c_{l,tors}$ defined as in the original DS model, cf. Equations (4) and (5).

The induced drag, which is based on the complete lift coefficient in the original model, Equation (7), is now only based on the circulatory lift component:

$$c_{d,ind} = c_{l,circ}(\alpha_{3/4} - \alpha_E) \tag{16}$$

Further a torsion rate drag component is added. This component accounts for AOA differences in the three quarter and quarter chord point due to the torsion rate. In Section 5.1 it is shown that this drag term cancels out the unphysical aerodynamic power at zero wind speed due to evaluating the AOA at the three quarter chord point and placing the lift force at the quarter chord point.

$$c_{d,tors} = c_{l,circ} T_0 \dot{\theta} \tag{17}$$

The total drag coefficient is:

$$c_d = c_{d,E} + c_{d,sep} + c_{d,ind} + c_{d,tors} \tag{18}$$

# 4 Force coefficient loops for VAWT operation at high wind speed

## 4.1 VAWT operation at high wind and resulting $c_l$ and $c_d$ loops

The following figures are results for operation of a H-type VAWT with 13.3 meter blade length and 9.85 meter rotor radius. The VAWT rotates at a constant 33 rpm and the incoming, uniform wind has a speed of 18 m/s. Results are from the middle section of the blades, where the chord length is 1.17 meters.

At these conditions, the geometric AOA varies between roughly -33 and +26.5 degrees during each rotation. The time series of AOA is shown in the left plot of Figure 1. During the increase of AOA, a maximum AOA rate of change of roughly 220 deg/s is reached. The right plot in Figure 1 contains the effective AOA, determined in the attached flow part of the dynamic stall model. The original model predicts a very large AOA lag, where the effective AOA is a maximum of 14 degrees behind the geometric AOA. This is because the angle of attack difference drives the attached flow timelag, independent of the flow state around the airfoil (attached, partial stall or deep stall). In the updated model, where the new contributions to the AOA lag are scaled with the separation function ($f_{sep}$=1 in fully attached, $f_{sep}$=1 in fully separated flow), the effective AOA is always within 3 degrees of the geometric AOA.

The lift and drag coefficient loops predicted by both original and updated model are shown in Figure 2. The lift coefficient loop in the original model has an extreme opening that has not been seen in measurements. The large AOA lag in the original model also leads to a large induced drag which is responsible for the large negative drag area in the $c_d$ loop.

The $c_l$ loop according to the updated model has a much smaller opening, and the drag coefficient only reaches slightly negative values.

The different contributions to the lift and drag coefficient loops will be evaluated in more detail in the following section.

## 4.2 Investigation of different contributions to $c_l$ and $c_d$ coefficients

The lift coefficient excluding the torsion rate and accelaration term is shown along with the fully separated and fully attached lift coefficient in Figure 3. The main differences between both models here is that the loops of the attached flow and separated flow curves are much more closed in the updated model due to the smaller effective AOA lag. Both original and updated model predict that the lift coefficient follows the attached flow curve on the way down. On the way from negative to positive AOAs, the rate of change of AOA is much larger (cf. Figure 1). Because of the large effective AOA lag in the original model the lift coefficient follows the separated curve until it starts attaching at a geometric AOA of roughly 15 degrees. In the updated model, due to the smaller AOA lag, attachment starts at roughly 0 degrees.

The torsion rate and acceleration components of the lift coefficient are shown in Figure 4. Only the torsion rate term was included in the original model (left plot). The added acceleration

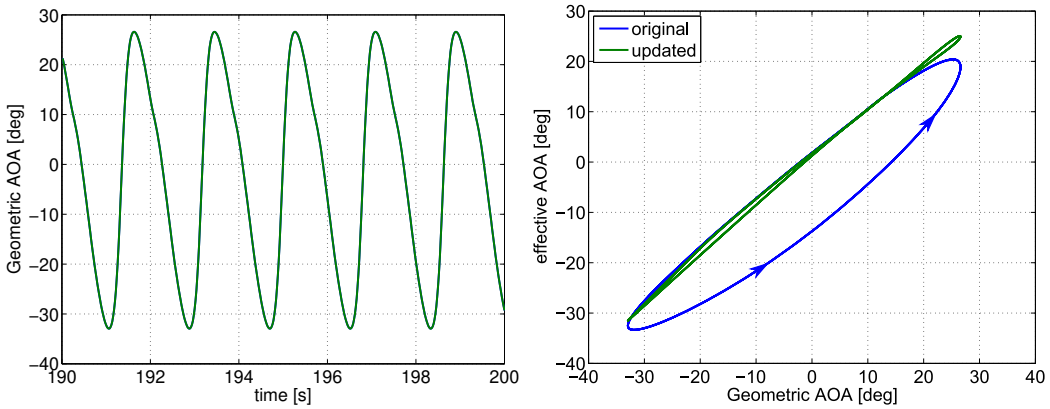


*Figure 1*: Left:Time series of geometric angle of attack during VAWT operation at high wind speed. Right: loops of effective angle of attack in original and updated model.

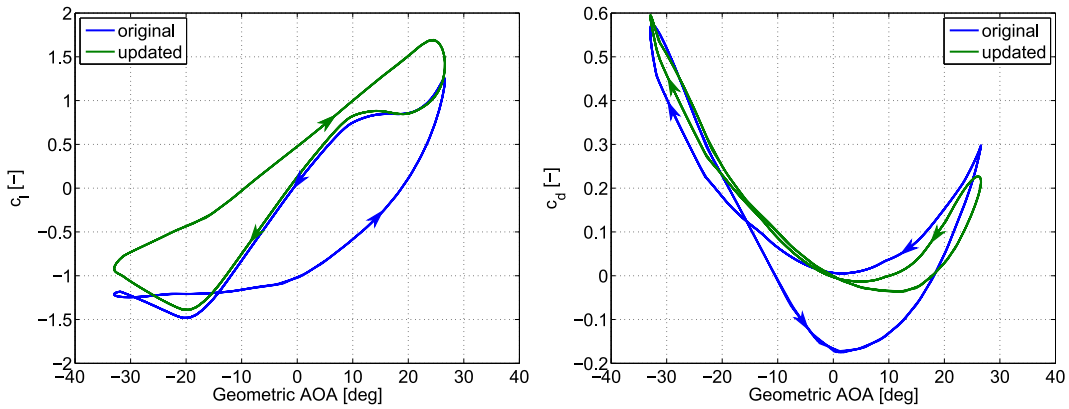


*Figure 2*: Loops of lift and drag coefficient during VAWT operation at 18 m/s wind speed.

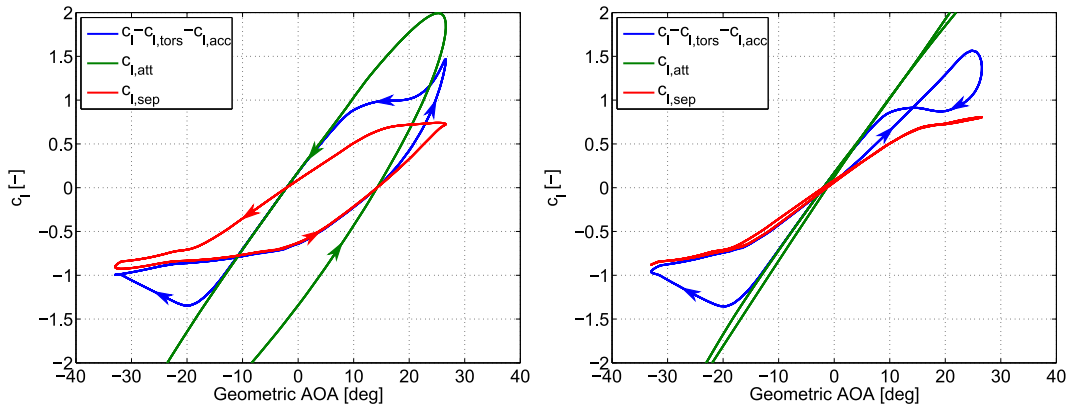


*Figure 3*: Attached and separated components of $c_l$ from original (left plot) and updated (right plot) dynamic stall model.

term in the updated model is shown to almost cancel out with the torsion rate term at high relative velocities (when the AOA decreases and CL follows the attached flow curve). At low relative velocities (increasing AOA) the acceleration term reaches almost a value of 0.8 and becomes much larger than the torsion rate term. Therefore the updated model predicts a higher lift coefficient when the AOA is on the way up, following the separated flow curve due to the high rate of change of the AOA, than when the angle of attack decreases and the lift coefficient follows the attached flow curve.

The different contributions to the drag coefficient are shown in Figure 5. This plot confirms that the large negative drag area predicted by the original model is due to the induced drag caused by the large effective angle of attack lag. The absolute value of the induced drag predicted by the updated model is much lower. The torsion rate contribution to the drag coefficient in the updated model reaches negative values at positive geometric AOA and pulls the drag coefficient down slightly below zero.

The normal and tangential force coefficient loops are shown in Figure 6. As expected, the normal force loops are very similar to the lift coefficient loops. The tangential force loop according to the updated model is closer to the 'butterfly' shaped loops obtained in experiments [4, 5].

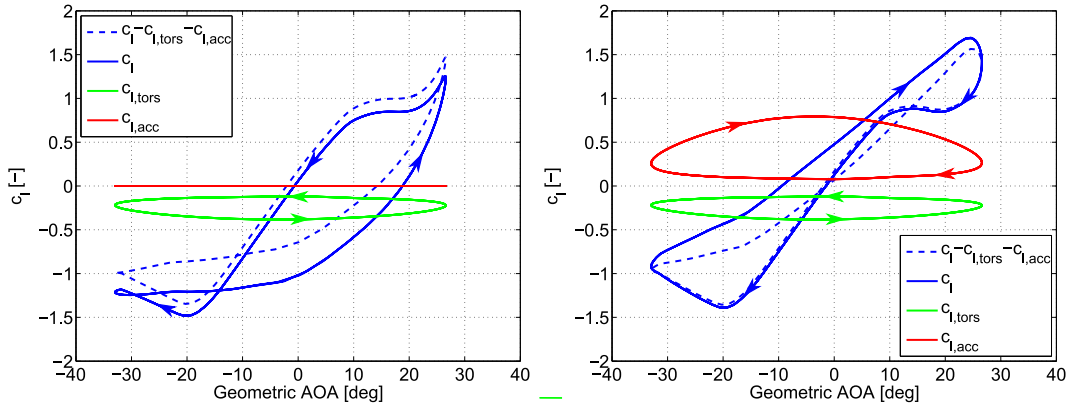


*Figure 4*: Complete lift coefficient and components due to torsion rate and acceleration from original (left plot) and updated (right plot) dynamic stall model.

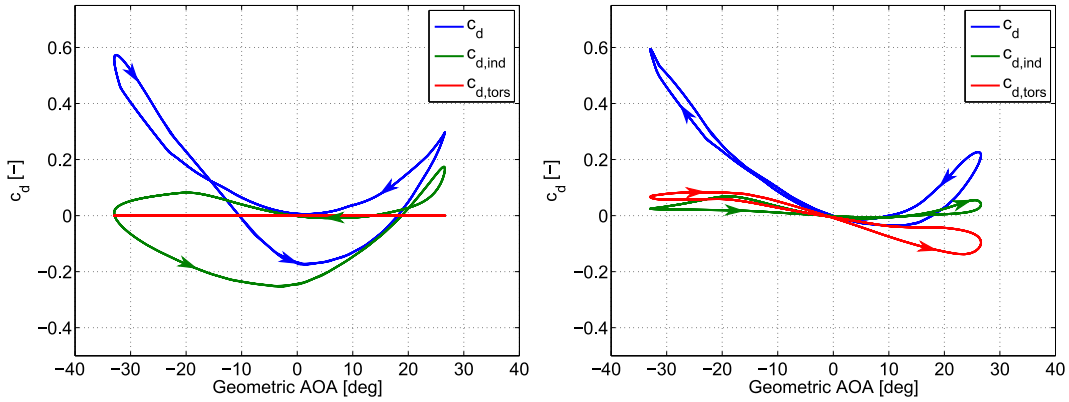


*Figure 5*: Complete drag coefficient, induced drag and drag due to torsion rate and acceleration from original (left plot) and updated (right plot) dynamic stall model.

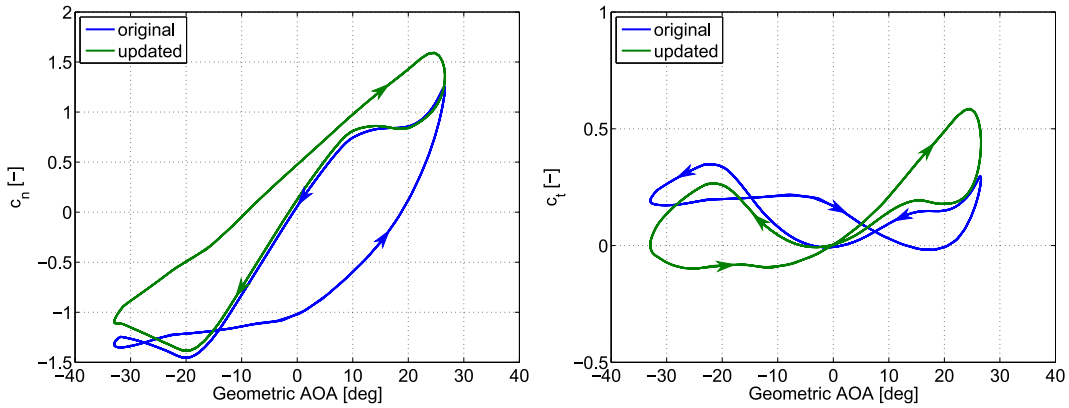


*Figure 6*: Loops of normal and tangential force coefficient during VAWT operation at 18 m/s wind speed.

# 5 VAWT at zero wind speed

There had been an issue with VAWTs producing power at zero wind speed when using the Beddoes-Leishman type dynamic stall model. In this section, it is shown that, for a VAWT at zero wind speed:

- the newly included acceleration lift term cancels out with the torsion rate lift term
- the driving moment due to the newly included torsion rate drag term cancels out with the moment due to the angle of attack evaluation at $3/4$ chord and lift application at the $1/4$ chord

Therefore, with the updated model, a VAWT produces exactly zero power at zero wind speed if a symmetric airfoil with no drag is used (as opposed to a positive power in the original model).

## 5.1 Canceling of acceleration and torsion rate lift terms

If the wind speed is 0, the torsion rate term and acceleration term in the lift coefficient will cancel out. In these conditions, the relative velocity is simply $\omega r$, the torsion rate is $-\omega$ and the acceleration at the mid chord is $-\omega^2 r$. It follows that:

$$c_{l,tors} = b\pi\frac{\dot{\theta}}{v_{rel}} = b\pi\frac{-\omega}{\omega r} = -\frac{b}{r}\pi \tag{19}$$

$$c_{l,acc} = -b\pi\frac{\ddot{y}}{{v_{rel}}^2} = -b\pi\frac{-\omega^2 r}{(\omega r)^2} = \frac{b}{r}\pi \tag{20}$$

Therefore, if only the torsion rate term is included in the computations, there would be a nonphysical constant lift component pulling the airfoil section forward (because the angle of attack is not zero if the calculation point is not exactly on the midchord) that would create a positive power at zero wind speed.

## 5.2 Canceling of moment around hub

A sketch of a simple H-rotor geometry is shown in Figure 7. The following analysis shows that the moments due to lift and torsion rate drag around the center of rotation cancel out. It is assumed that $\alpha$, the AOA at the three quarter chord point due to the rotation, is small. Thus the moment arm for the lift is $b\cos\alpha \approx b$ and the moment arm for the drag is $r/(\cos\alpha) - b\sin\alpha \approx r$.

The angle of attack at the three quarter chord point is:

$$\alpha = \frac{b}{2r} \tag{21}$$

$$\tag{22}$$

The lift coefficient is, assuming a symmetric airfoil:

$$c_l = 2\pi\alpha \tag{23}$$

$$c_l = \pi\frac{b}{r} \tag{24}$$

$$\tag{25}$$

The moment due to the lift force is found as:

$$M_L = \frac{\rho}{2}v_{rel}^2 c_l b = \frac{\rho}{2}v_{rel}^2\pi\frac{b^2}{r} \tag{26}$$

$$\tag{27}$$

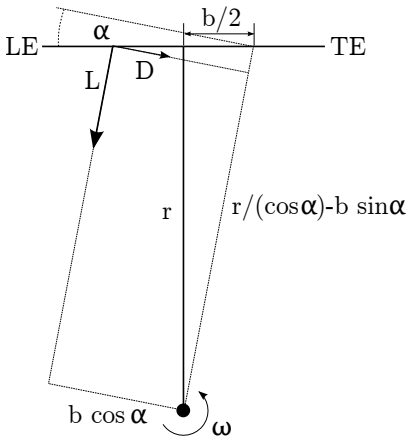


*Figure 7*: Sketch of geometry at one blade of an H rotor rotating.At zero wind speed, the AOA at the three quarter chord point and thus lift and drag directions depend only on the geometry: on the rotor radius $r$ and the half chord $b$.

Similarly follows for the moment due to the torsion rate drag:

$$c_d = -c_l \frac{\dot{\theta} b}{v_{rel}} = \pi \frac{b}{r} \frac{-\omega b}{\omega r} = \pi \frac{b^2}{r^2} \tag{28}$$

$$M_D = -\frac{\rho}{2} v_{rel}^2 c_d r = -\frac{\rho}{2} v_{rel}^2 \pi \frac{b^2}{r^2} r = -\frac{\rho}{2} v_{rel}^2 \pi \frac{b^2}{r} = -M_L \tag{29}$$

Thus both moments cancel out, and an H-rotor with an airfoil with no airfoil drag ($c_{d,polar} = 0$) will produce zero power when rotating at zero wind.

Because the torsion rate drag coefficient is proportional to the lift coefficient, the same conclusion holds for cambered airfoils.

# 6 Validation on a pitching blade in standstill against original model and measurements

- Comparison of results from original and modified model against measurements of the pitching NREL/NASA Ames Phase VI blade in standstill, [6]
- Influence of the model modifications is generally small
- Influence tends to be in the right direction when it comes to the opening of the loop
- Acceleration term can become problematic for 'stiff' blades that might undergo small movements at very high frequencies. These movements would otherwise not affect the aerodynamic forces.
- Differences are partly due to missing induction modeling at standstill, partly due to difficulties modeling deep stall and partly due to measurement uncertainty.

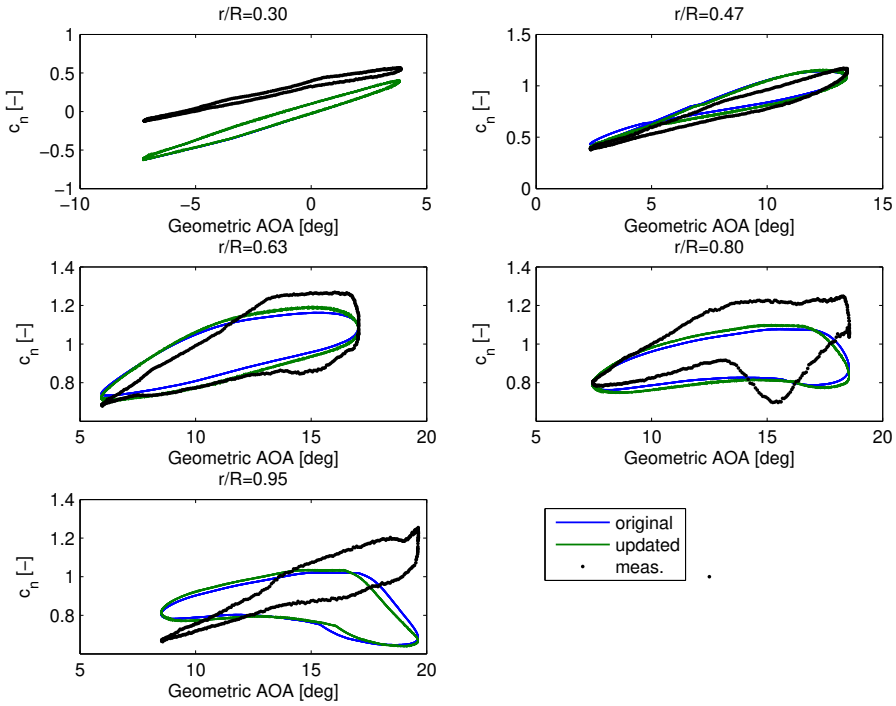


*Figure 8*: Loops of normal force coefficient for a pitching blade in standstill. Mean AOA at 47% radius: 7.91 degrees, pitching time 0.8496 s, pitching amplitude 5.55 deg.

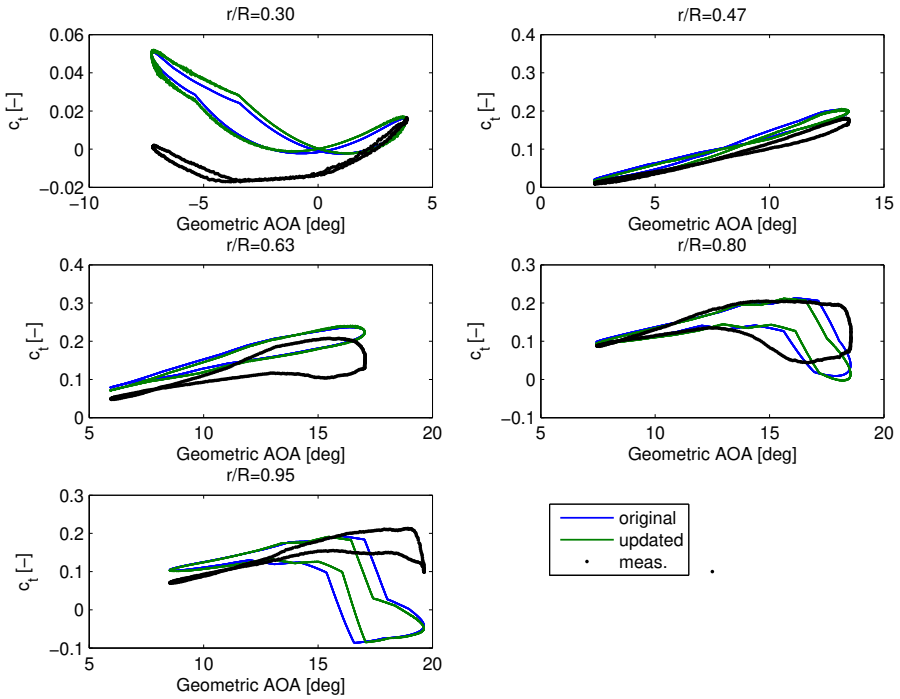


*Figure 9*: Loops of tangential force coefficient for a pitching blade in standstill. Mean AOA at 47% radius: 7.91 degrees, pitching time 0.8496 s, pitching amplitude 5.55 deg.

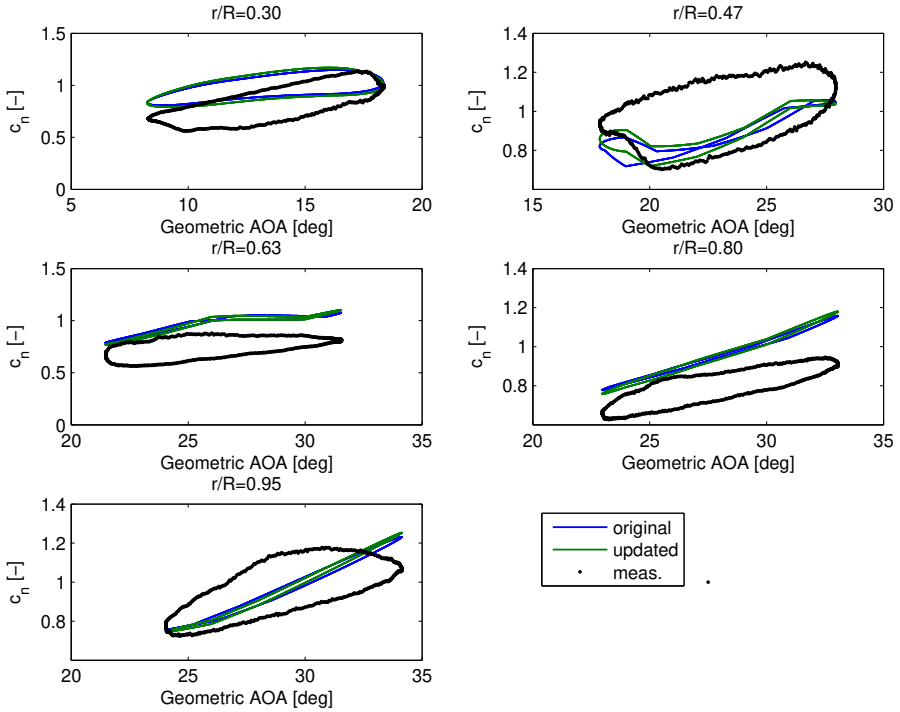


*Figure 10*: Loops of normal force coefficient for a pitching blade in standstill. Mean AOA at 47% radius: 22.92 degrees, pitching time 1.1261 s, pitching amplitude 5.04 deg.

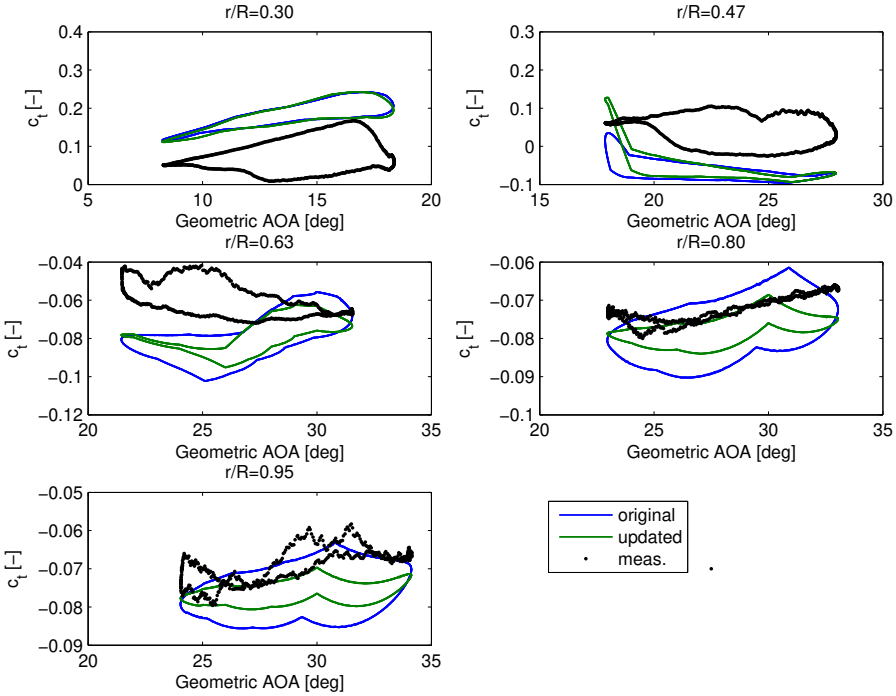


*Figure 11*: Loops of tangential force coefficient for a pitching blade in standstill. Mean AOA at 47% radius: 22.92 degrees, pitching time 1.1261 s, pitching amplitude 5.04 deg.

# 7 Conclusions

- The additional torsion rate and acceleration terms eliminate the power production at zero wind speed.
- The modified attached flow indicial function algorithm reduces the previously very large angle of attack lags at high wind speed.
- The modifications combined lead to much more reasonably looking lift and drag loops at high wind speed.
- The influence of these modifications on the power curve prediction is currently being investigated.
- The effect of the modifications on small loops at varying mean AOA is generally found to be small. These conditions are typical for HAWT operation and thus the effect of the modifications on HAWT in normal operation is small.

# References


[1] M. H. Hansen, M. Gaunaa, and H. Aa. Madsen. *A Beddoes-Leishman type dynamic stall model in state-space and indicial formulations*. Risø-R-1354, Roskilde, Denmark, 2004.

[2] Leonardo Bergami and Mac Gaunaa. *ATEFlap Aerodynamic Model, a dynamic stall model including the effects of trailing edge flap deflection*. Danmarks Tekniske Universitet, Ris Nationallaboratoriet for Bredygtig Energi, 2012.

[3] Peter Bæk. *Unsteady Flow Modeling and Experimental Verification of Active Flow Control Concepts for Wind Turbine Blades*. PhD thesis, 2011.

[4] Frank Schuerich and Richard E Brown. Effect of dynamic stall on the aerodynamics of vertical-axis wind turbines. *AIAA journal*, 49(11):2511–2521, 2011.

[5] Eduard Dyachuk, Anders Goude, and Hans Bernhoff. Dynamic stall modeling for the conditions of vertical axis wind turbines. *AIAA journal*, 52(1):72–81, 2013.

[6] Niels N. Srensen and Scott Schreck. Computation of the national renewable energy laboratory phase-vi rotor in pitch motion during standstill. *Wind Energy*, 15(3):425–442, 2012.

**Technical University of Denmark**
**DTU Vindenergi**

**info@vindenergi.dtu.dk**
**www.vindenergi.dtu.dk**